Analysis and Applications of a General Boresight Algorithm for the DSS-13 Beam Waveguide Antenna

L. S. Alvarez
Ground Antennas and Facilities Engineering Section

A general antenna beam boresight algorithm is presented. Equations for axial pointing error, peak received signal level, and antenna half-power beamwidth are given. A pointing error variance equation is derived that illustrates the dependence of the measurement estimation performance on the various algorithm inputs, including RF signal level uncertainty. Plots showing pointing error uncertainty as a function of algorithm inputs are presented. Insight gained from the performance analysis is discussed in terms of its application to the areas of antenna controller and receiver interfacing, pointing error compensation, and antenna calibrations. Current and planned applications of the boresight algorithm, including its role in the upcoming Ka-band downlink experiment (KABLE), are highlighted.

I. Introduction

Antenna beam boresigthing algorithms were developed in 1990 for gain and pointing calibrations carried out during the DSS-13 beam waveguide (BWG) Antenna Phase 1 Project[1]. The three- and five-point algorithms are currently implemented on a personal computer (PC) that interfaces with both the antenna radiometer systems and the antenna mechanical system to close an RF loop around the pointing system. At the present time, these algorithms are being moved to the antenna mechanical system as part of a planned DSS-13 controller upgrade that is to be a prototype for future DSN antenna controllers (e.g., the new DSS-24 BWG antenna). The boresighting program will obtain the input signal level from receivers over the station local area network (LAN). Specifically, system noise temperature estimates will be received from the total power radiometer subsystem and coherent SNR estimates will be obtained from the TP-13 and Advanced Receiver II (ARX) subsytem.

This article will present the general boresight algorithm. As part of the new implementation, an equation describing the propagation of signal level input measurement uncertainty into axial pointing errors was derived and is presented here. The signal level uncertainty can be the sum of numerous ground antenna sources as noise and/or errors from the antenna front-end electronics and measurement devices, antenna servo errors, as well as incident (coherent) signal dynamics due to spacecraft attitude controls and varying downlink modulation indices. It will be shown that the pointing error variance equation also to

[1] M. J. Britcliffe, L. S. Alvarez, D. A. Bathker, P. W. Cramer, T. Y. Otoshi, D. J. Rochblatt, B. L. Seidel, S. D. Slobin, S. R. Stewart, W. Veruttipong, and G. E. Wood, *DSS 13 Beam Waveguide Antenna Project: Phase 1 Final Report*, JPL D-8451 (internal doc-

sighting performance based on the (assumed random and independent) RF SNR measurements and also on other system parameters (e.g., antenna half-power beamwidth, pointing error magnitudes, etc.). Plots that illustrate the dependence of the algorithm performance on the numerous input variables will be given. Insight gained from the performance analysis will be discussed in terms of antenna controller and receiver interfaces, pointing error compensation, and pointing calibrations. The article will also highlight some of the current and planned applications of the algorithm, including its utilization in the upcoming Ka-band downlink experiment (KABLE).

II. Boresight Algorithm

Three- and five-point boresight algorithms applicable to tracking extragalactic radio sources were developed and programmed in 1990 by R. Riggs. The algorithms map measured on- and off-source noise temperature measurements into estimates of axial (cross-elevation and elevation) pointing error, peak temperature, and antenna half-power beamwidth (full-width). The algorithms continue to be successfully applied at DSS 13 to boresight the BWG antenna, that is, maintain the peak of the antenna beam aligned with the target during gain and pointing calibration sessions. Details of the current PC-based implementation and usage can be found in Footnote 1 and [1,2]. The general algorithm will be presented below in such a manner as to not be dependent on any specific receiver for signal level input.

This particular boresighting scheme is actually a step scan that measures signal level at small angles off-boresight along a single axis at a time. A five- (or three-) point boresight implies that five (or three) measurements on-source along an axis are input into the algorithm. In the case of noncoherent signal inputs, the on-source measurements are obtained by using two off-source measurements to negate contribution of the baseline cold-sky system noise. The data points are then fit to a linearized exponential to yield desired pointing and peak received power estimates. Five- and three-point step scans will be implemented in the DSS-13 antenna pointing system, but in general any finite number (greater than two) of signal level measurements can comprise the input. The default offsets where measurements are taken are points that correspond to the 3-dB, 1-dB, and 0-dB points on both sides of the beam relative to the assumed true direction of the target. The three-point version has default offsets corresponding to measurements at the 1-dB (both sides) and peak-signal levels. Arbitrary offsets can be used but their magnitudes are bound by the validity of the Gaussian model used to approximate the antenna beam pattern.

Let the signal level inputs (in linear units) be $y_i, i = 1, \ldots, n$, sensed at the angular offsets $x_i, i = 1, \ldots, n$ superimposed on the predicted target angles, then the received signal level model is

$$y_i(x_i) = y_{peak} \exp\left(-\frac{4\ln(2)}{H^2}(x_i - \varepsilon)^2\right) \tag{1}$$

where y_{peak} is the peak signal level at boresight, H is the antenna (full-width) half-power beamwidth, and ε is the pointing error. These three variables are calculated by the algorithm. The solution involves solving for the coefficients c_1, c_2, and c_3 of the best-fit parabola satisfying the set of n equations

$$\ln\left(y_i(x_i)\right) = c_1 + c_2 x_i + c_3 x_i^2 \tag{2}$$

or

$$y_i(x_i) = \exp\left(c_1 + c_2 x_i + c_3 x_i^2\right) \tag{3}$$

By differentiating Eq. (3) with respect to x and equating to zero, the offset corresponding to peak signal level, that is, the pointing error ε, is determined to be

$$\varepsilon = -\frac{c_2}{2c_3} \tag{4}$$

Now, since y_{peak} is defined to be $y(\varepsilon)$ by Eq. (3), the peak signal level is found to be

$$y_{peak} = \exp\left(c_1 - \frac{c_2^2}{4c_3}\right) \tag{5}$$

Finally, by equating Eqs. (1) and (3), and setting the angular offset x arbitrarily to zero, the solution equation for the half-power beamwdith can be solved to be

$$H = \sqrt{-\frac{4\ln(2)}{c_3}} \tag{6}$$

In general, the coefficients c_1, c_2 and c_3 are calculated via the method of least squares from the set of n equations defined by Eq. (2). However, in the case where $n = 3$, the three coefficients can be solved for directly from the set of three equations obtained from Eq. (2).

III. Variance Propagation

The computed values of ε, y_{peak}, and H will have uncertainties σ_ε, $\sigma_{y_{peak}}$, and σ_H due to the measurement errors in the signal level inputs y_i, and perhaps due to significant antenna position errors in the offsets x_i. An equation describing the propagation of the uncertainties in the signal level inputs into axial pointing errors, assuming negligible position offset errors, will be presented below. If needed in the future, similar variance equations can be derived for the efficiency variables y_{peak} and H.

The measurement function in Eq. (2) is ln (y_i). Let $y_{\ln_i} = \ln(y_i)$, and let the uncertainty in the signal level inputs y_i be σ_{y_i}, then the measurement uncertainty in $y_{\ln_i}$ is

$$\sigma_{y\ln_i} = \frac{\sigma_{y_i}}{y_i} \tag{7}$$

and will be propagated through the boresight algorithm. The σ_{y_i}'s are also presumed to encompass all uncertainty that was introduced in negating cold-sky background noise from the y_i. For example, in the classic two-point method of removing the background sky noise contribution in order to isolate the target signal levels, the resultant variance on y_i is increased as described in Appendix B.

Now, assuming negligible uncertainty in the x_i and that the $\sigma_{y\ln_i}$ are random and independent, then the variance of the computed pointing error ε is

$$\sigma_\varepsilon^2 = \sum_{i=1}^{n} \left(\frac{\partial \varepsilon}{\partial y_{\ln_i}} \sigma_{y\ln_i} \right)^2 \tag{8}$$

From the pointing error solution Eq. (4), the following partial derivative equation is obtained:

$$\frac{\partial \varepsilon}{\partial y_{\ln_i}} = \frac{1}{2c_3^2} \left(c_2 \frac{\partial c_3}{\partial y_{\ln_i}} - c_3 \frac{\partial c_2}{\partial y_{\ln_i}} \right) \tag{9}$$

which can be inserted into Eq. (8) to yield

$$\sigma_\varepsilon^2 = \left(\frac{1}{2c_3^2} \right)^2 \sum_{i=1}^{n} \left(c_2 \frac{\partial c_3}{\partial y_{\ln_i}} - c_3 \frac{\partial c_2}{\partial y_{\ln_i}} \right)^2 \sigma_{y\ln_i}^2 \tag{10}$$

where c_1, c_2 and c_3 are the best fit coefficients from Eq. (2). From Eq. (6), c_3 can be written in terms of the half-power beamwidth H as

$$c_3 = -\frac{4 \ln (2)}{H^2} \tag{11}$$

and then substituting c_3 into the pointing error Eq. (4) yields

$$c_2 = (2\varepsilon) \frac{4 \ln (2)}{H^2} \tag{12}$$

Both of the above two equations along with the noise to signal Eq. (7) can now be inserted into Eq. (10) to write the pointing error variance in terms of the boresight algorithm input variables. Inserting and simplifying yield

$$\sigma_\varepsilon^2 = \left(\frac{H^2}{8 \ln (2)} \right)^2 \sum_{i=1}^{n} \left(2\varepsilon \frac{\partial c_3}{\partial y_{\ln_i}} + \frac{\partial c_2}{\partial y_{\ln_i}} \right)^2 \left(\frac{\sigma_{y_i}}{y_i} \right)^2 \tag{13}$$

Further expansion of the partial derivatives of c_2 and c_3 is given in Appendix A. As seen from Eq. (13) the accuracy of ε depends, in general, on a number of factors: the noise-to-signal ratio (NSR) of the target, the antenna half-power beamwidth H, and the magnitude of the actual pointing error ε being estimated. As illustrated in Appendix A, the magnitude of the axial offsets x_i also impacts σ_ε through the partial derivative equations of c_2 and c_3. Performance in terms of these parameters will be illustrated in the following section.

Two subtle effects that can also degrade estimation accuracy of ε are large, simultaneous pointing errors in each axis and inordinate signal integration time. Large errors in the axis perpendicular to the one where ε is being computed will increase σ_ε through a decrease in signal level y_i (which increases the NSR) in Eq. (13). This may or may not be a major concern, depending on the particular application of the boresight algorithm and the quality of the pointing calibration of the antenna. For example, gain and pointing calibration applications minimize this effect by continuously measuring and correcting ε sequentially in each axis.

Long signal integration times combined with the significant antenna servo move delays may result in axial step scan measurement periods on the order of minutes or longer. The sidereal motion of the antenna can then result in a smearing-type degradation on ε. This is especially true if the antenna is in a poor calibration state where pointing errors can quickly build up as a function of antenna orientation.

Careful interpretation should be applied to computed values of σ_ε during practical DSN tracking operations.

Specifically, the pointing error variance equation was derived assuming that the input noise to signal measurements σ_{y_i}/y_i are independent and random. This assumption does not hold, for example, when the received signal error sources include drifts and/or biases induced by incident signal dynamics from spacecraft attitude controls and varying downlink modulation indices.

IV. Performance Analysis and Applications

A. Performance

Performance of the boresight algorithm can be expressed in terms of the output pointing error standard deviation σ_ϵ with respect to the various inputs. In the following, the performance of the algorithm will be quantified with respect to a 34-m antenna at both X-band (8.45 GHz) and Ka-band (32 GHz) frequencies (i.e., the half-power beamwidths are 65 and 17 mdeg, respectively). An important statistic is the target NSR, or standard deviation σ_{yln_i} defined by Eq. (7). Figure 1 shows a plot of σ_ϵ versus σ_{yln_i} for both three- and five-point boresight algorithms. The uncertainties were calculated with offsets corresponding to a zero pointing error. The signal losses corresponding to both five-point and three-point algorithms are the same for X- and Ka-bands, and are shown in Fig. 2 for the zero pointing error case. As seen, irrespective of frequency, the five-point algorithm is less sensitive to input noise.

Estimation uncertainty in a single axis also increases with the magnitude of the pointing error ε. Figures 3 and 4 illustrate this effect for the five-point algorithm at the Ka- and X-band frequencies, respectively. As seen, σ_ϵ increases dramatically with ε at Ka-band, while with the same error magnitudes at X-band it is essentially insensitive. The antenna beam-pointing error vector is defined as the rss of the simultaneous errors sensed in the elevation and cross-elevation axes. Thus, the true performance of the algorithm is two-dimensional. Figure 5 shows how ε varies while estimating zero error with an increasing pointing error in the opposite axis. Here σ_y/y is chosen to be 0.03 for all five signal inputs. This is a typical NSR observed during low wind (less than 16.7 km/hr) radio source measurement periods at DSS 13. As seen, the Ka-band two-axes performance can be significantly degraded if large errors are present in the perpendicular axis. The X-band performance is basically insensitive to the cross-axis error due to the larger beamwidth. Figure 6 shows the cross-offset Ka-band effect on the five-point algorithm as a function of NSR for the zero pointing error case and Fig. 7 summarizes its two-axes Ka-band performance with

B. Antenna Controller and Receiver Interfaces

The antenna pointing system controller interfaces with radiometers and receivers. With respect to the implementation of the boresight algorithm, signal level integration times can be specified based on required pointing estimate accuracy, as shown in the plots of σ_ϵ against input noise to signal levels. The design can be based on worst-case expected receiver SNR, or the signal levels can be integrated (at the receiver or the antenna controller) with an adaptive integration time until a specified input σ_{yln} is achieved. Estimates of the signal level variances need to be processed simultaneously with the magnitude estimates for input into the boresight algorithm. The equations that process the measurement variance estimates from the DSS-13 total power radiometer and TP-13 and ARX II receiver subsystems are presented in Appendix B.

C. Pointing Error Compensation

The boresight algorithm is typically used solely for antenna calibration and alignment tasks. However, it will be utilized as a beam-pointing error compensation mechanism for the upcoming KABLE at DSS 13. The plan is to blind point the antenna at the Mars Observer Spacecraft and use three- or five-point boresights to periodically peak the received signal by negating any residual pointing error buildup. The goal is to have the antenna in the best possible pointing calibration state so as to maximize time between boresights and thus avoid the received signal losses associated with the off-peak axial measurements taken at the offsets x_i. The pointing error variances will allow real-time assessment of the computed axial corrections before their application.

During KABLE, the spacecraft will provide a simultaneous X-/Ka-band downlink. If the antenna X- and Ka-band beams are coaligned, it is possible to utilize either of the two signals for the pointing error compensation. With respect to the input NSR, Fig. 1 indicates that the X-band signal needs to be considerably stronger than the Ka-band in order to achieve the same pointing estimation performance. This is especially true with the expectation that DSS 13 will be in a highly calibrated state for KABLE, since Fig. 7 illustrates that the Ka-band performance is still superior when estimating small pointing errors.

D. Pointing Calibrations

The formal computation of a pointing error variance during pointing measurements is novel in the DSN. In addition to adding a real-time performance assessment capability during calibration tracks, the pointing uncertainties

analysis and pointing error modeling. It is anticipated that a more accurate antenna pointing calibration can be obtained from a now-possible weighted least-squares estimate of the pointing model coefficients.

Figures 3 through 7 also give some pointing calibration insight for Ka-band applications. When possible, it is best to first calibrate the antenna (or a particular focal point) at a lower frequency (e.g., X-band) to take out the large pointing errors. As illustrated, the larger X-band 34-m antenna beamwidth yields an increased insensitivity of the boresight uncertainty with respect to pointing error magnitudes. Figure 7 suggests, without considering the actual SNR conditions, that calibrating with the 34-m Ka-band signal should commence when the pointing errors are brought down to the 5.0- to 6.0-mdeg level. For comparison, Figs. 8 and 9 show the boresight estimation performance of the 34- and 70-m antennas with a 0.0- and 5.0-mdeg error in both the measurement axis and cross-axis, respectively.

V. Summary

A general antenna beam boresight algorithm has been presented. Although three- and five-point algorithms were analyzed for the current DSS-13 antenna controller upgrade, the equations derived for pointing error, peak received signal and antenna half-power beamwidth are general. A variance equation, which maps signal level measurement uncertainty into axial pointing errors, was derived. It is also being implemented in the DSS-13 upgrade. This is the first time that pointing error measurement uncertainties will be formally computed in a DSN or DSN research antenna. Plots were presented that illustrate the dependence of the pointing error estimation performance on the numerous input variables. In general, for the 34-m antenna, the algorithm with Ka-band input will outperform the X-band input case with respect to input SNR, assuming that the errors being estimated, as well as cross-axis errors, are at or below 5.0 mdeg. The Ka-band performance is dramatically degraded as these pointing errors increase.

Current and planned applications of the boresight algorithm and pointing error variance equation were discussed. Signal level input variance equations specific to the DSS-13 antenna controller interface with the total power radiometer and TP-13 and ARX II receiver subsystems were given in Appendix B. The boresight performance analysis presented will aid in future antenna controller/receiver interface and pointing error compensation designs. The availability of pointing error measurement uncertainties will enhance off-line antenna performance analysis and calibration efforts. The planned application of the algorithm for pointing error compensation in the upcoming KABLE was also highlighted.

Acknowledgments

Christian Sanelli is acknowledged for his assistance in deriving the pointing error variance equation. Hemali Vyas, who is currently implementing the boresight algorithm in the DSS-13 antenna controller, provided many insightful discussions on a practical level. A previous uncertainty analysis of a six-point parabolic cross-scan algorithm by J. C. Breidenthal provided useful technical direction.

References

[1] S. D. Slobin, T. Y. Otoshi, M. J. Britcliffe, L. S. Alvarez, S. R. Stewart, and M. M. Franco, "Efficiencey Calibration of the DSS 13 34-Meter Beam Waveguide Antenna at 8.45 and 32 GHz," *TDA Progress Report 42-106*, vol. April–June 1991, Jet Propulsion Laboratory, Pasadena, California, pp. 283–297, August 15, 1991.

[2] L. S. Alvarez, "Initial Pointing Calibrations for the DSS 13 34-Meter Beam-Waveguide Antenna," *TDA Progress Report 42-106*, vol. April–June 1991, Jet Propulsion Laboratory, Pasadena, California, pp. 188–204, August 15, 1991.

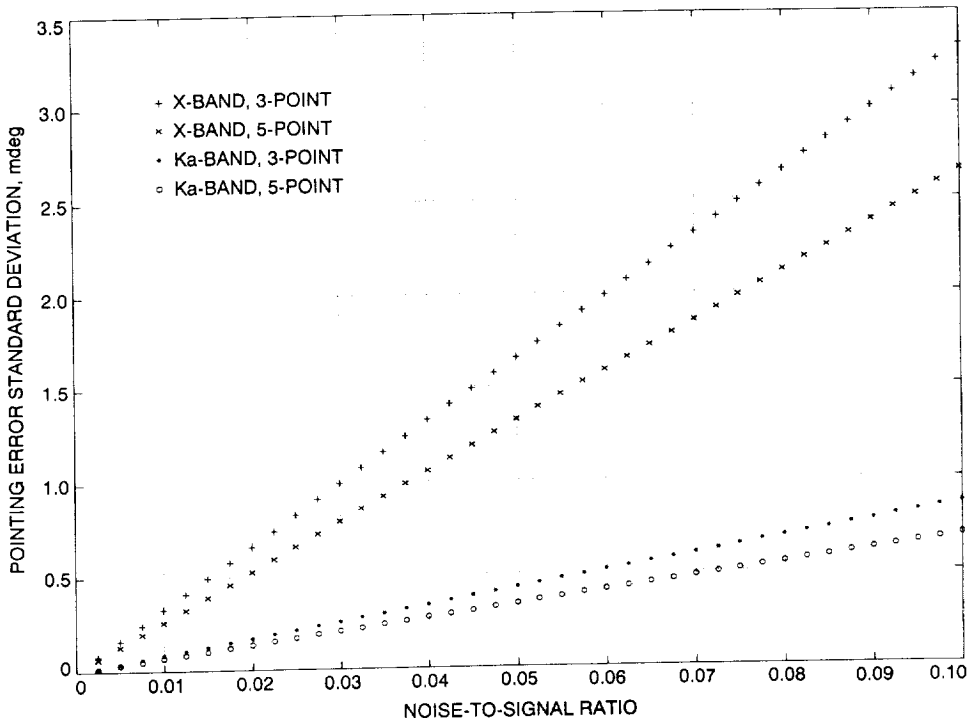

Fig. 1. Boresight uncertainty analysis for zero pointing error case.

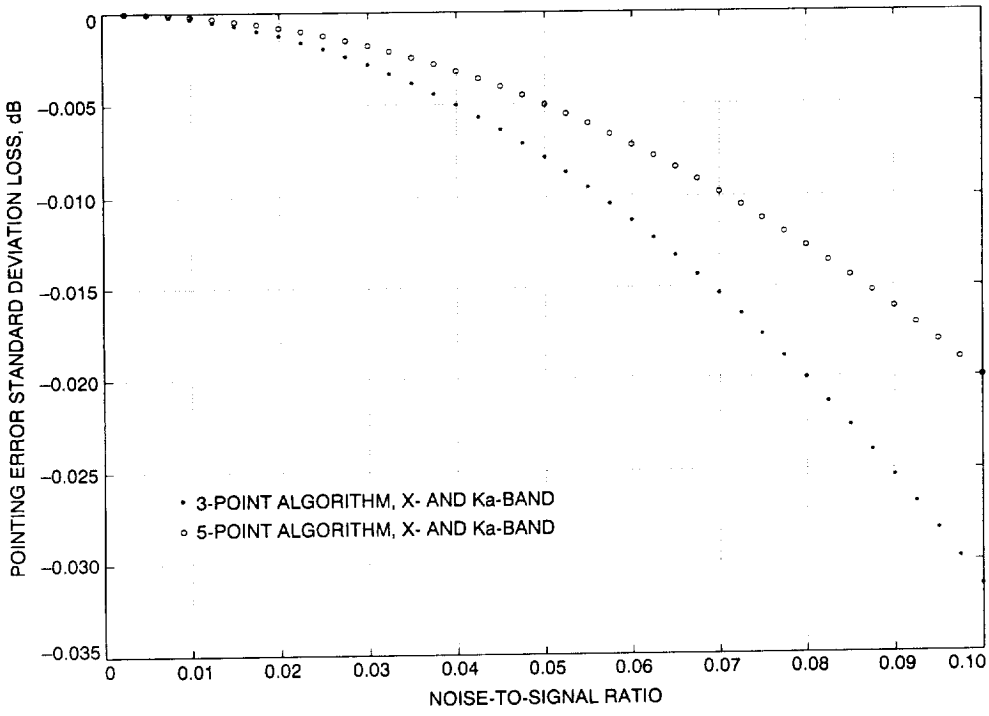

Fig. 2. Boresight error uncertainty loss for zero pointing error case.

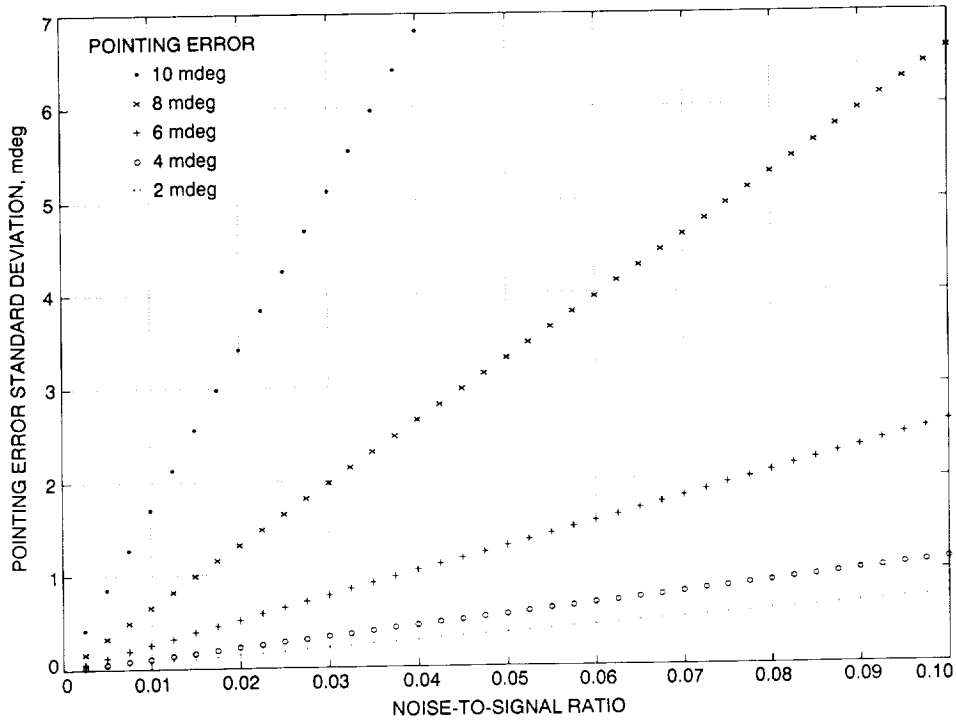

Fig. 3. Ka-band 5-point boresight uncertainty for increasing pointing errors.

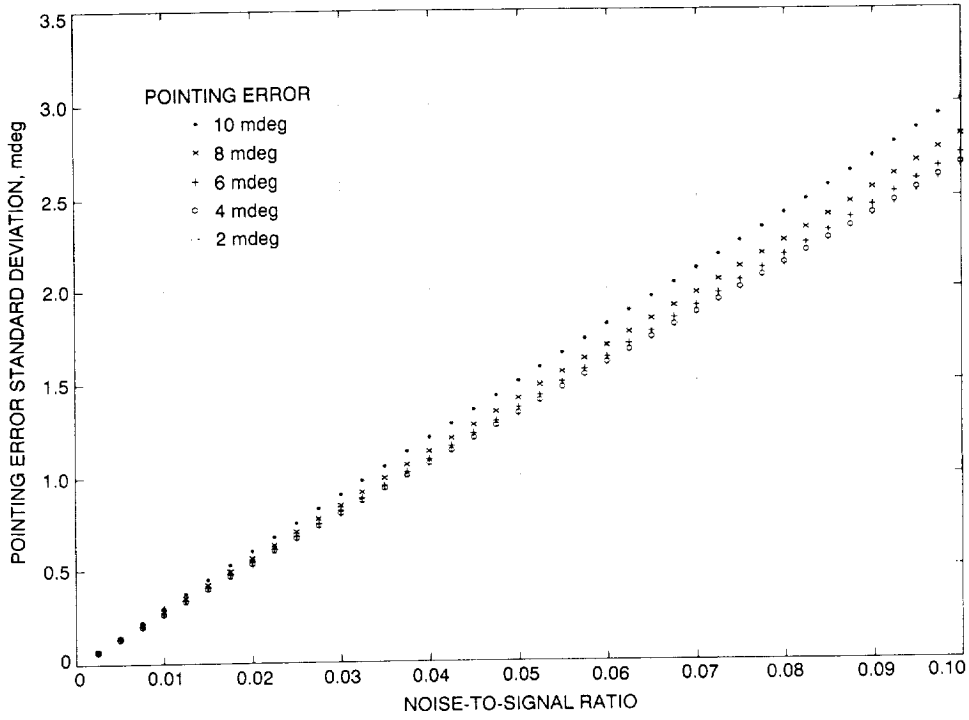

Fig. 4. X-Band 5-point boresight uncertainty for increasing pointing errors.

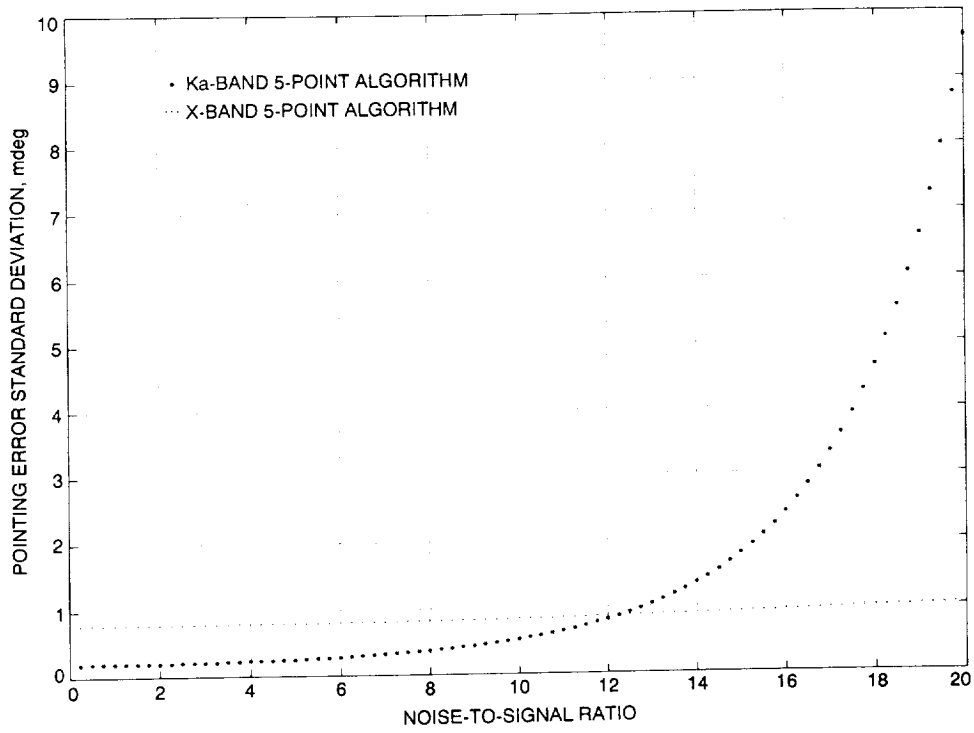

Fig. 5. Five-point boresight uncertainty for increasing cross-axis errors with NSR of 0.03, zero pointing error case.

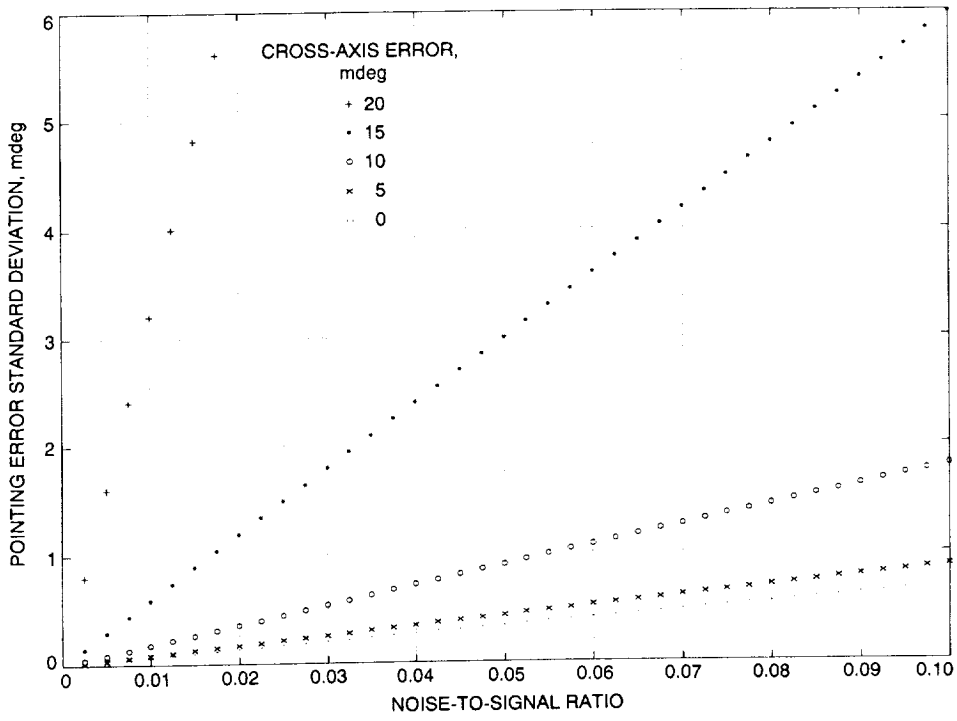

Fig. 6. Ka-band 5-point boresight uncertainty for increasing cross-axis errors, zero pointing error case.

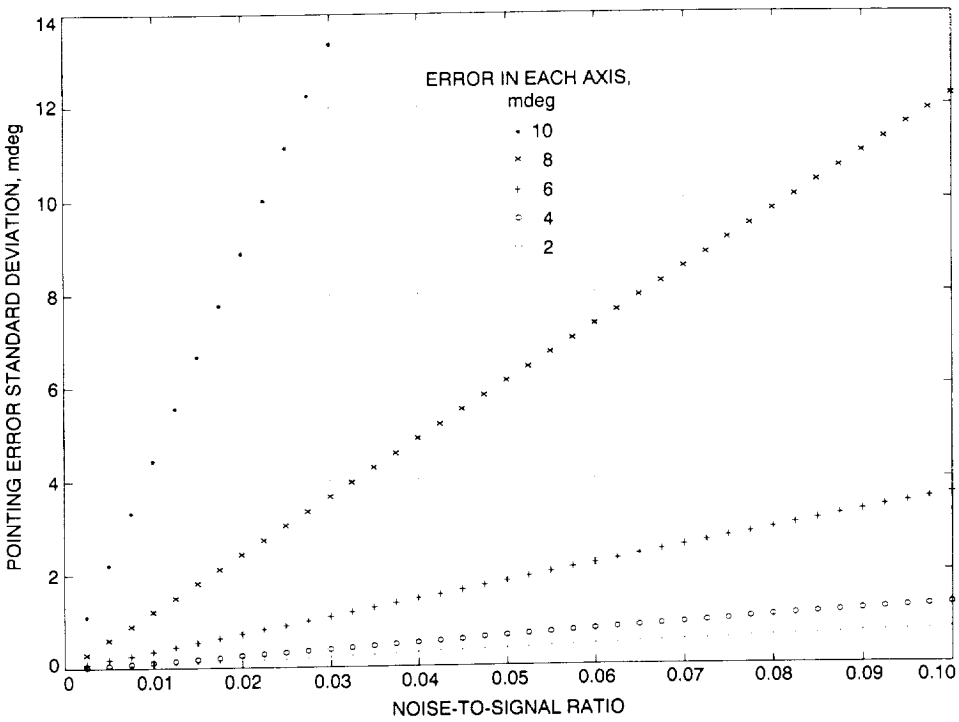

Fig. 7. Ka-band 5-point boresight uncertainty for equally increasing pointing and cross-axis errors.

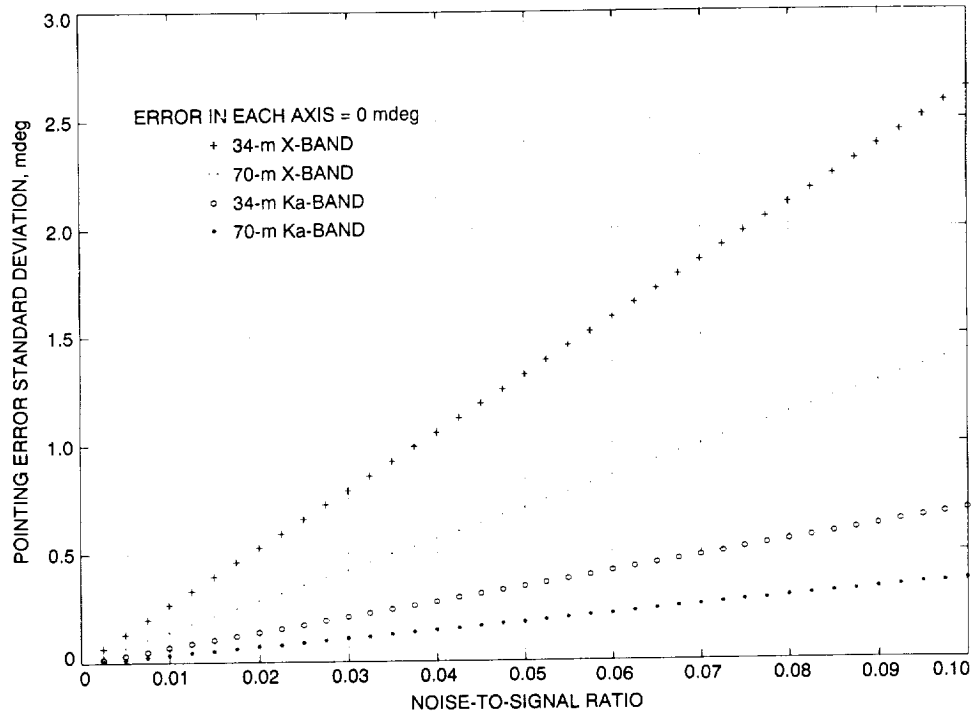

Fig. 8. 5-point boresight uncertainty for zero pointing and cross-axis errors.

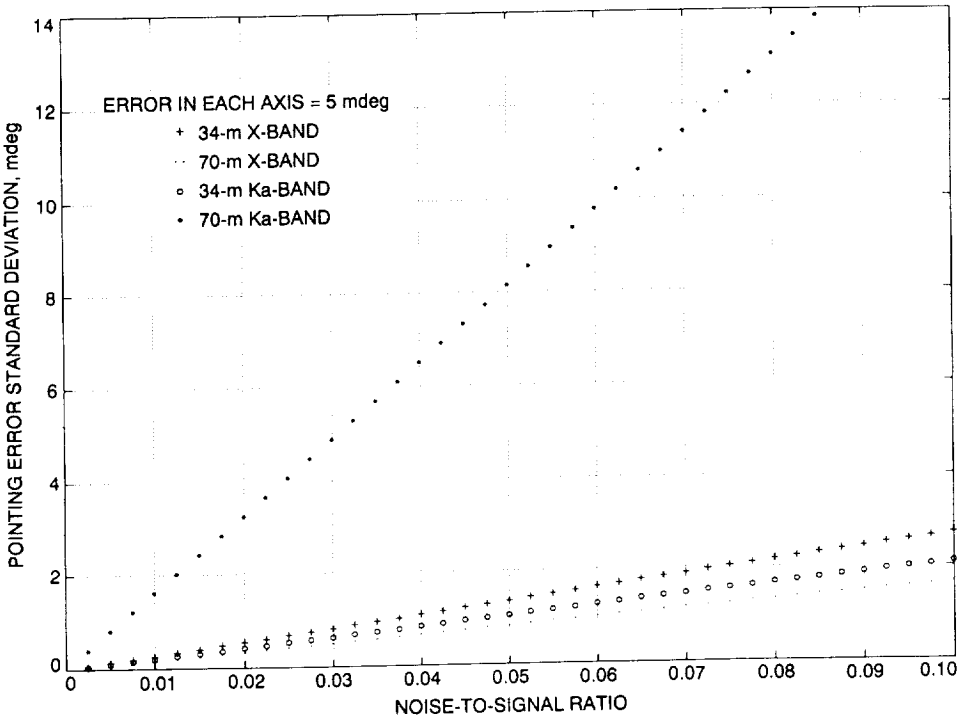

Fig. 9. 5-point boresight uncertainty for equal pointing and cross-axis errors of 5.0 mdeg.

Appendix A

Pointing Error Variance Equation

Let the signal level inputs be $y_i, i = 1, \ldots, n$, that are sensed at the angular offsets $x_i, i = 1, \ldots, n$ superimposed on the predicted target angles, then the received signal level model can be written in the following exponential form:

$$y_i(x_i) = \exp\left(c_1 + c_2 x_i + c_3 x_i^2\right) \tag{A-1}$$

It can be shown that the offset where the signal level is maximum, i.e., where $x = \varepsilon$ and ε is the beam pointing error, is

$$\varepsilon = -\frac{c_2}{2c_3} \tag{A-2}$$

where c_i, $i = 1, \ldots, 3$ are the coefficients of the best fit parabola satisfying the set of n equations

$$\ln\left(y_i\left(x_i\right)\right) = c_1 + c_2 x_i + c_3 x_i^2 \tag{A-3}$$

or in matrix notation

$$\begin{bmatrix} \ln\left(y_1\right) \\ \vdots \\ \ln\left(y_n\right) \end{bmatrix} = \begin{bmatrix} 1 & x(1) & x(1)^2 \\ & \vdots & \\ 1 & x(n) & x(n)^2 \end{bmatrix} \begin{bmatrix} c_1 \\ c_2 \\ c_3 \end{bmatrix} \tag{A-4}$$

which can be written as

$$\mathbf{Y_{ln}} = \mathbf{AC} \tag{A-5}$$

where the measurement vector $\mathbf{Y_{ln}}$ is $n \times 1$, the measurement distribution matrix $\mathbf{A}$ is $n \times 3$, and the parameter vector $\mathbf{C}$ is 3×1. The computed value of the pointing error from Eq. (A-2) will have an uncertainty σ_ε due to measurement errors in the signal level inputs y_i, and perhaps due to significant antenna position errors in the offsets x_i.

The measurement function in Eq. (A-3) is $\ln\left(y_i\right)$. Let $y_{ln_i} = \ln\left(y_i\right)$, and the uncertainty in the signal level inputs y_i be σ_{y_i}, then the measurement uncertainty in y_{ln_i} is

$$\sigma_{y_{ln_i}} = \frac{\sigma_{y_i}}{y_i} \tag{A-6}$$

and will be propagated through the boresight algorithm. The σ_{y_i} are also presumed to encompass all uncertainty that was introduced in negating cold sky background noise from the y_i. Now, assuming negligible uncertainty in the x_i and that the $\sigma_{y_{ln_i}}$ are random and independent, then the variance of the computed pointing error ε is

$$\sigma_\varepsilon^2 = \sum_{i=1}^{n} \left(\frac{\partial \varepsilon}{\partial y_{ln_i}} \sigma_{y_{ln_i}}\right)^2 \tag{A-7}$$

From the pointing error solution Eq. (A-2), the following partial derivative equation is obtained:

$$\frac{\partial \varepsilon}{\partial y_{ln_i}} = \frac{1}{2c_3^2}\left(c_2 \frac{\partial c_3}{\partial y_{ln_i}} - c_3 \frac{\partial c_2}{\partial y_{ln_i}}\right) \tag{A-8}$$

which can be inserted into Eq. (A-7) to yield

$$\sigma_\varepsilon^2 = \left(\frac{1}{2c_3^2}\right)^2 \sum_{i=1}^{n} \left(c_2 \frac{\partial c_3}{\partial y_{ln_i}} - c_3 \frac{\partial c_2}{\partial y_{ln_i}}\right)^2 \sigma_{y_{ln_i}}^2 \tag{A-9}$$

Analytic expressions for $\partial c_2 / \partial y_{ln_i}$ and $\partial c_3 / \partial y_{ln_i}$ are needed to completely describe the variance Eq. (A-9). The least squares solution for the vector $\mathbf{C}$ satisfies the following matrix equation:

$$\mathbf{C} = \left(\mathbf{A}^\mathbf{t}\mathbf{A}\right)^{-1} \mathbf{A}^\mathbf{t} \mathbf{Y_{ln}} \tag{A-10}$$

where $\mathbf{A}^\mathbf{t}$ is the transpose of $\mathbf{A}$. Let the the matrix product $\left(\mathbf{A}^\mathbf{t}\mathbf{A}\right)$ be denoted as $\mathbf{D}$ and be expanded [from Eq. (A-4)] as

$$\begin{bmatrix} d_{11} & d_{12} & d_{13} \\ d_{21} & d_{22} & d_{23} \\ d_{31} & d_{32} & d_{33} \end{bmatrix} = \begin{bmatrix} n & \sum x_i & \sum x_i^2 \\ \sum x_i & \sum x_i^2 & \sum x_i^3 \\ \sum x_i^2 & \sum x_i^3 & \sum x_i^4 \end{bmatrix} \tag{A-11}$$

where all summations (from here on) are from $i = 1$ to n. Let $\mathbf{D}'$ be the inverse of the matrix $\mathbf{D}$, or $\mathbf{D}' = \mathbf{D}^{-1}$ where

$$\mathbf{D}' = \begin{bmatrix} d'_{11} & d'_{12} & d'_{13} \\ d'_{21} & d'_{22} & d'_{23} \\ d'_{31} & d'_{32} & d'_{33} \end{bmatrix} \quad \text{(A-12)}$$

From Eq. (A-10) it can be shown that the solutions for c_2 and c_3 are

$$c_2 = d'_{21} \sum y_{ln_i} + d'_{22} \sum x_i y_{ln_i} + d'_{23} \sum x_i^2 y_{ln_i} \quad \text{(A-13)}$$

and

$$c_3 = d'_{31} \sum y_{ln_i} + d'_{32} \sum x_i y_{ln_i} + d'_{33} \sum x_i^2 y_{ln_i} \quad \text{(A-14)}$$

Finally, from the last two solution equations the needed partial derivative equations are calculated to be

$$\frac{\partial c_2}{\partial y_{ln_i}} = d'_{21} + d'_{22} x_i + d'_{23} x_i^2 \quad \text{(A-15)}$$

and

$$\frac{\partial c_3}{\partial y_{ln_i}} = d'_{31} + d'_{32} x_i + d'_{33} x_i^2 \quad \text{(A-16)}$$

and can be inserted in Eq. (A-9) to complete the pointing error variance equation.

Appendix B

DSS-13 Signal Level Input Variance Propagation Equations

The new DSS-13 antenna mechanical controller, called the antenna monitor and control computer (AMC), will interface with both the total power radiometer and TP-13 and ARX II receiver subsystems for noncoherent and co-

[redacted]

appendix will summarize the signal level variance propagation equations needed for each of the interfaces. It is noted that the boresight algorithm input is required to be in linear units, as opposed to logarithmic units proportional to power typically used to describe RF power measurments.

I. Noncoherent Signal Input

AMC inputs from the total power radiometer subsystem will be estimates of system noise temperature T_i with their standard deviations σ_{T_i} measured at the on-source angular offsets x_i, $i = 1, \ldots, n$, and the two off-source measurements T_{off1} and T_{off2} with their standard deviations $\sigma_{T_{off1}}$ and $\sigma_{T_{off2}}$ sensed at the offsets x_{off1} and x_{off2}. This axial measurement scheme is depicticed in Fig. B-1 for the case of $n = 3$, i.e., the three-point boresight algorithm. The required input to the boresight algorithm are the source noise temperature estimates T_{source_i} with variances $\sigma^2_{T_{source_i}}$ corresponding to the x_i. The classic straight-line sky background noise approximation is used to isolate the target signal levels. The following equation is applied to estimate the off-source background sky temperatures T_{sky_i} along the line shown in Fig. B-1:

$$T_{sky_i} = a_i(T_{off2} - T_{off1}) + T_{off1} \quad for\ i = 1, \ldots, n \quad \text{(B-1)}$$

where

$$a_i = \frac{abs(x_i - x_{off1})}{abs(x_{off2} - x_{off1})} \quad \text{(B-2)}$$

and then, assuming that all of the temperature variances are independent and random, the estimated sky variances from (B-4) are

$$\sigma^2_{T_{sky_i}} = (1 - a_i)^2\sigma^2_{T_{off1}} + a_i^2\sigma^2_{T_{off2}} \quad \text{(B-5)}$$

where a_i is defined above. Finally, from Eq. (B-3) the source signal level variances are obtained as

$$\sigma^2_{T_{source_i}} = \sigma^2_{T_i} + \sigma^2_{T_{sky_i}} \quad \text{(B-6)}$$

and T_{source_i} and $\sigma^2_{T_{source_i}}$ for $i = 1, \ldots, n$ are the required inputs for the boresight algorithm and pointing error variance equation.

II. Coherent Signal Input

AMC inputs from the TP-13 and ARX II receiver subsystems will be estimates of SNR's $(P_c/N_o)_i$ and variances $\sigma^2_{(P_c/N_o)_i}$ sensed at the on-source angular offsets x_i. Estimates of noise power $(N_o)_i$ and variances $\sigma^2_{(N_o)_i}$ will be derived from simultaneous radiometer subsystem inputs of system noise temperatures T_i and standard deviations σ_{T_i} measured at the on-source angular offsets x_i. The noise power estimates over a 1-Hz bandwidth are defined as $(\hat{N}_o)_i = \kappa T_i$, where κ is Boltzmann's Constant. Then the estimated noise power variances are then $\sigma^2_{(\hat{N}_o)_i} = \kappa^2\sigma^2_{T_i}$. Multiplication negates the noise power from the target signal power, as follows:

$$(\hat{P}_c)_i = \left(\frac{P_c}{N_o}\right)_i (\hat{N}_o)_i \quad \text{(B-7)}$$

[redacted]

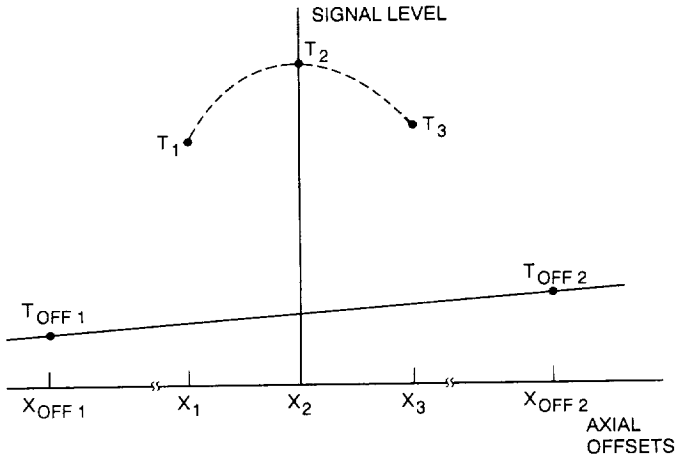

Fig. 10. Noncoherent signal measurement scheme.